IEEE Access
Multidisciplinary | Rapid Review | Open Access Journal

Received April 19, 2020, accepted April 30, 2020, date of publication May 4, 2020, date of current version May 19, 2020.

Digital Object Identifier 10.1109/ACCESS.2020.2992346

Optimization of a Fuze MEMS Setback Arming Device Based on the EDM Process

YU QIN[1], LIANGYU CHEN[1], AND YONGPING HAO[2]
[1]School of Mechanical Engineering and Automation, Northeastern University, Shenyang 110819, China
[2]School of Mechanical Engineering, Shenyang Ligong University, Shenyang 110159, China

Corresponding author: Yu Qin (qinyu490@163.com)

ABSTRACT This paper introduces the working principle of a MEMS safety and arming (S&A) device and measures and tests a setback arming device. To solve the problem of large fabrication errors in the UV-LIGA process, a MEMS S&A fuze device fabricated by low-speed wire electrical discharge machining (EDM) is proposed. Microsprings are susceptible to flexural deformation and secondary deformation in the EDM process, which is solved by setting the auxiliary support beam, using multiple cuts and destress annealing. The linewidth, thickness and elastic coefficient of the microspring fabricated using the EDM process are closer to the designed values than those fabricated using the UV-LIGA process under the same conditions. When comparing the MEMS S&A devices fabricated by the two processes, it is found that the EDM process has a the higher machining accuracy. In view of the plastic deformation of the upper end of the microspring, the structure of the microspring is optimized to incorporate a gradient linewidth, and the optimized setback arming device is tested. The results show that the device can ensure service process safety and launch reliability. The maximum overload that can be withstood in service processing is 17000 g, and the minimum overload for insurance release during launch is 1500 g.

INDEX TERMS Fuze, MEMS safety and arming device, UV-LIGA process, EDM process, microspring.

I. INTRODUCTION

In recent years, with the development of MEMS technology, the application of this technology in a fuze has gained attention [1]–[8]. Miniaturization and intelligentization of the traditional mechanical fuze is difficult due to its large size and heavy components. A MEMS fuze is designed with a flat plate structure, which has the advantages of a small size, low mass and high reliability. This structure is an important direction for future fuze development [9]–[12]. As an important structure of fuze MEMS safety and arming (S&A) devices, the setback arming device is the key factor to ensure service processing safety and launch reliability [13]–[15]. Many researchers have carried out a great deal of work in modeling, simulation analysis and reliability analysis of the fuze MEMS setback arming device. Dakui *et al.* [16] studied the influence of the microspring elastic coefficient on the release insurance time of a MEMS setback arming device through theoretical calculations and simulation analysis. The conclusion was that the microspring elastic coefficient has little effect on the time required for the setback slider to move to the released position. Tu *et al.* [17] put forward a method of structural reliability simulation based on the finite element method and its realization process. A quantitative reliability analysis of a fuze MEMS setback arming device was carried out, and the problem of ''automatic call'' of the finite element software tool in the reliability analysis was solved. Seok *et al.* [18] proposed a ball-driven-type MEMS setback arming device, introduced the design process of the device and carried out a simulation analysis and experimental verification of the device. The results showed that the ball-driven MEMS setback arming device had appropriate safety and arming performance. There has been little research on the fabrication process of MEMS S&A devices; most researchers use the DRIE (deep reactive ion etching) process, LIGA process or UV-LIGA process to fabricate these devices [19]–[22]. These methods have many limitation, such as process complexity, high processing costs, large fabrication errors and long processing times [23]–[28]. These problems constrain the device structure and the extension of the function and the development of engineering applications of MEMS S&A devices. In this paper, the fabrication process

The associate editor coordinating the review of this manuscript and approving it for publication was Sanket Goel.

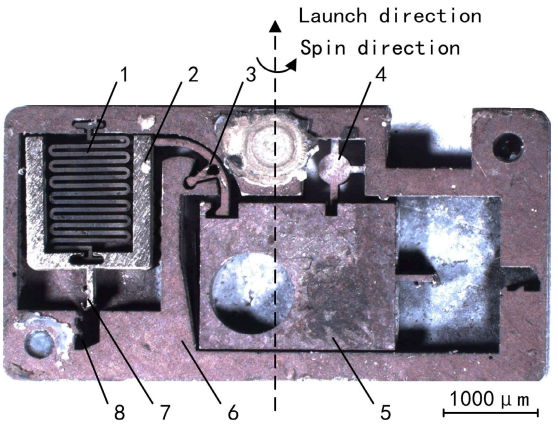

FIGURE 1. Fuze MEMS S&A device. 1-Microspring, 2-setback slider, 3-rotary pin, 4-shear pin, 5-arming slider, 6-frame, 7-head latch, 8-cassette latch.

and the microspring structure of a MEMS setback arming device are optimized, and the device, which is fabricated by the EDM process instead of the UV-LIGA process, is shown to offer high precision, low cost and batch production. The safety and reliability of the MEMS setback arming device can be guaranteed by optimizing the structure of the microspring into a gradient linewidth microspring. These optimization methods are of great significance for the engineering application of fuse MEMS S&A devices.

II. WORKING PRINCIPLE OF THE FUZE MEMS S&A DEVICE

Fig. 1 shows an assembled fuze MEMS S&A device consisting of a microspring, a setback slider, a rotary pin, a shear pin, an arming slider, a frame, a head latch and a cassette latch. The device is made of Ni using a UV-LIGA process, and its size is 13.3 mm × 7 mm × 0.65 mm. It is primarily used in medium- and large-diameter grenades and is placed parallel to the grenade shaft. The frame is tightly connected with the setback slider at the initial moment by a microspring. During a normal launch, the projectile is propelled by gunpowder gas in the chamber, which produces a high acceleration and causes the setback arming device to be subjected to a setback force. Under the action of the setback force, the setback slider overcomes the resistance of the microspring and the downward friction force between the slider and the frame until the head latch is locked in the cassette latch, and the first insurance is released. When the projectile passes through the rifle, it develops a large rotational speed, which causes the S&A device to experience a centrifugal force. When the centrifugal force reaches a certain value, the rotary pin rotates a specific angle counterclockwise under the action of the centrifugal force, which releases the first limit of the arming slider. When the projectile flies beyond the safe distance of the muzzle, the electric pin pusher starts to operate under the control of the delay circuit, shears the shear pin and releases the second limit of the arming slider. The arming slider then continues to move to the right under the continuous action of the centrifugal force until it is locked by the cassette latch, and the second insurance is released. At this moment, the MEMS S&A device insurance is fully released, the explosive train is aligned, and the fuze is in the pending state.

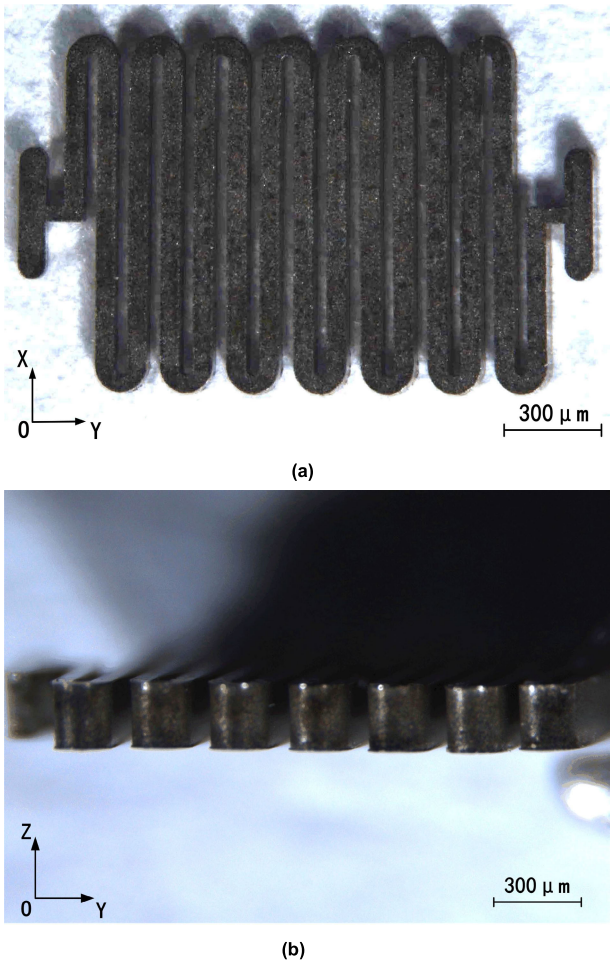

FIGURE 2. EMS micrograph of the microsprings. (a) Linewidth; (b) thickness.

III. TESTING OF THE SETBACK ARMING DEVICE

A. MEASUREMENT RESULTS

The microspring is an important component to ensure the safety of the fuze MEMS S&A device in normal time and its reliable function after launching. Fig. 2 shows an EMS photograph of the linewidth and thickness of the microspring in the setback arming device. Due to the fabrication error of the UV-LIGA process, the spring is uneven in linewidth and thickness. The designed value of the aspect ratio of the microsprings is 5:1. Fifty microsprings are used to measure the linewidth and thickness of each section. When taking the average of the measured values as the measured result of the spring, as shown in Fig. 3, the measured values of the linewidth and thickness are all found to be smaller than the designed values. This outcome is due to the corrosion error in the process of fabricating the microsprings by the UV-LIGA process [29]–[32]. By constructing a curve from

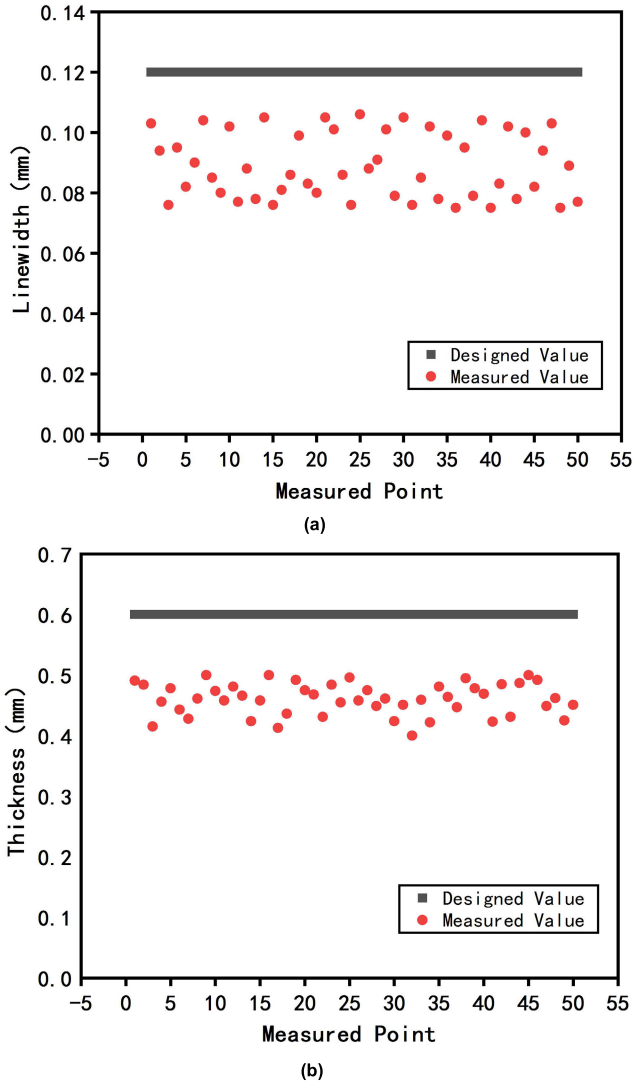

FIGURE 3. Measurement results. (a) Linewidth; (b) thickness.

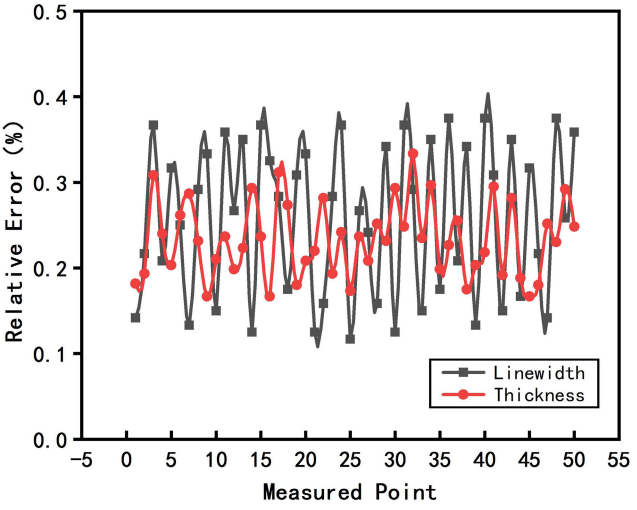

FIGURE 4. Relative error curve.

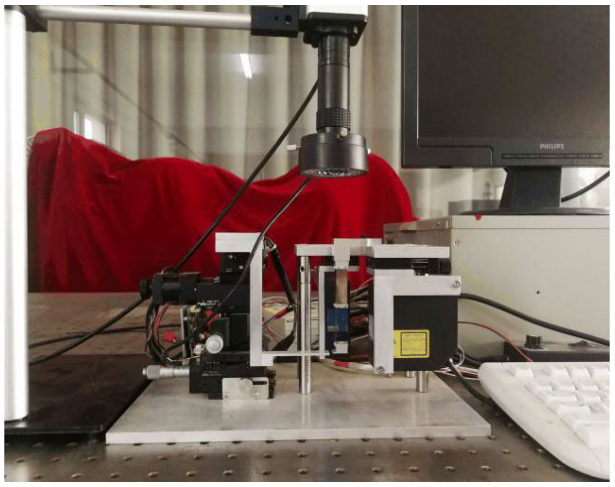

FIGURE 5. Photograph of the microspring testing system.

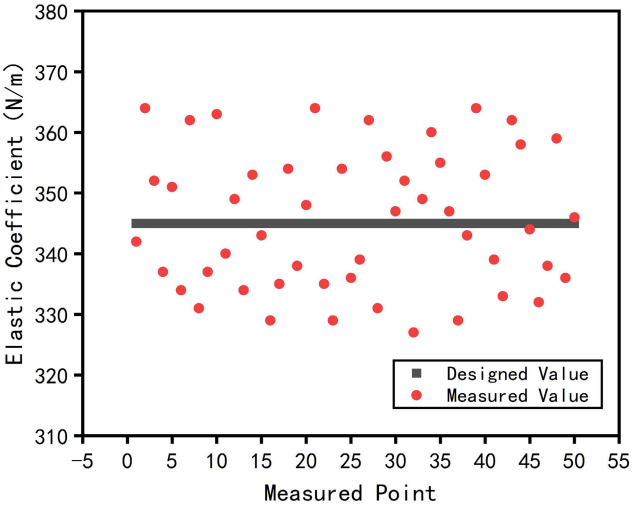

FIGURE 6. Elastic coefficient test results.

the relative error value between the measured value and the designed value, as shown in Fig. 4, the change amplitude of the relative error curve of the linewidth measurement value is found to be larger than that of the thickness, indicating that the error in the linewidth direction is larger. This is because for a microspring with a large aspect ratio, it takes longer to remove SU-8 glue in the thickness direction than in the linewidth direction when using the inorganic acid etching method, resulting in excessive linewidth etching.

Fig. 5 shows a high-precision microspring elastic coefficient testing system [33]. Fifty microsprings are tested by using the system, and the test results of the elastic coefficient are shown in Fig. 6. The results in Fig. 3 and Fig. 6 show that the measured values of the linewidth and the thickness of the microspring are smaller than the designed values, but the measured values of the elastic coefficient fluctuate around the designed values, indicating that the elastic coefficient of the microspring depends not only on the linewidth and thickness but also on the length of the straight beam, the spacing of the straight beam and the bending radius. This outcome is consistent with the conclusions in [34].

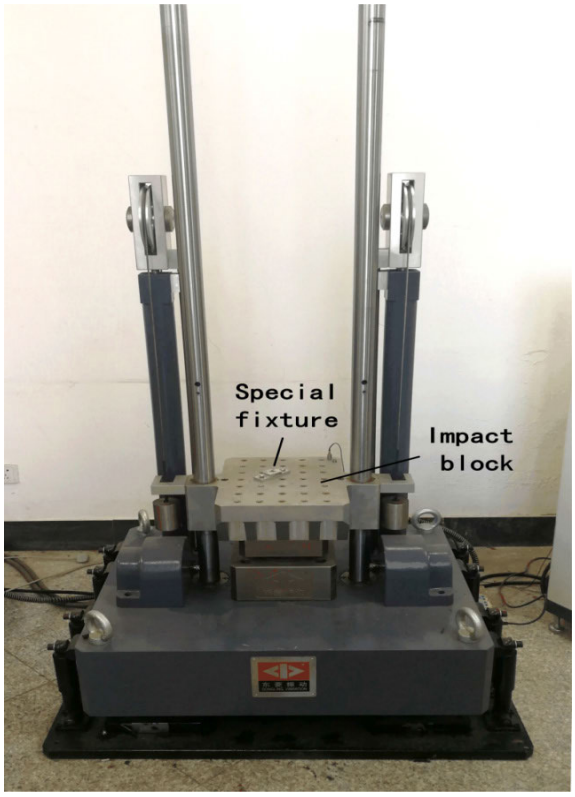

FIGURE 7. Impact test bench.

B. MECHANICAL IMPACT TEST RESULTS

To investigate the safety of the most dangerous cases in service processing, mechanical impact tests were carried out on the setback arming device. The technical indexes of the mechanical impact test include the impact waveform, impact acceleration and pulse duration [35]. A half sinusoidal pulse with a duration of 200 μs and a peak value at 100 μs was used to simulate the setback acceleration environment during service processing. Fig. 7 shows the impact test bench used in the test. Ten MEMS S&A devices were used for the test. Before the test, a special fixture was used to fix the device vertically on the test bench. During the test, the height of the impact block was adjusted to obtain impact accelerations of different magnitudes. The position of the setback slider was observed using a high-speed camera, and the test results are shown in Table 1. Plastic deformation occurred in all the microsprings of the setback arming device in the impact test. When the peak acceleration decreased from 20000 g to 15000 g, the head latch was locked by the cassette latch and could not return to the initial position. When the peak acceleration decreased from 14000 g to 11000 g, the head latch could not enter the cassette latch, and the plastic deformation of the microspring caused the setback slider to fail to return to the initial position under the action of the spring restoring force; at that time, the insurance was released. The mechanical impact test results show that the setback arming device cannot guarantee the safety of service processing.

Fig. 8 shows an SEM image of the setback arming device at the peak accelerations of 15000 g and 14000 g, in which a large plastic deformation occurred at the upper end of the microspring, while the rest of the springs were almost unchanged. Similar results were also observed in relevant tests conducted by Liu and Li [36], Liu *et al.* [37], and Li [38], and they have not yet provided effective solutions. This is because the stress distribution range of the microspring under the high overload impact is 360∼650 MPa, the fabrication error of the microspring makes the stress distribution of each section of the spring uneven, and the upper end of the spring is easy to produce a stress concentration. The material of the microspring is nickel, and its yield strength is 539 MPa.

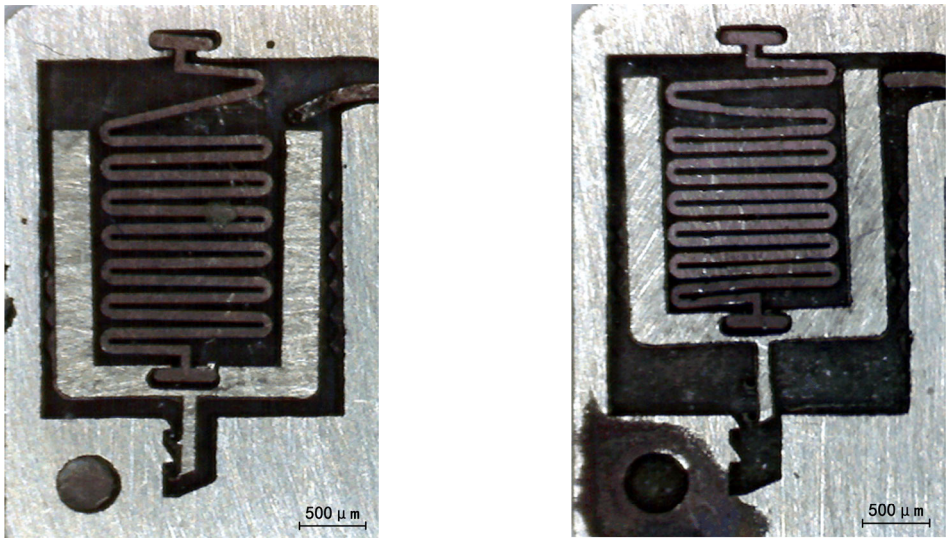

(a) (b)

FIGURE 8. Mechanical impact test results. (a) Peak acceleration of 15000 g; (b) peak acceleration of 14000 g.

TABLE 1. Mechanical impact test results.

Sample number	Peak acceleration /g	Head latch position	Deformation of microspring
1	20000	The head latch is locked by the cassette latch	Plastic deformation
2	19000	The head latch is locked by the cassette latch	Plastic deformation
3	18000	The head latch is locked by the cassette latch	Plastic deformation
4	17000	The head latch is locked by the cassette latch	Plastic deformation
5	16000	The head latch is locked by the cassette latch	Plastic deformation
6	15000	The head latch is locked by the cassette latch	Plastic deformation
7	14000	The head latch cannot enter the cassette latch and fail to return to the initial position	Plastic deformation
8	13000	The head latch cannot enter the cassette latch and fail to return to the initial position	Plastic deformation
9	12000	The head latch cannot enter the cassette latch and fail to return to the initial position	Plastic deformation
10	11000	The head latch cannot enter the cassette latch and fail to return to the initial position	Plastic deformation

TABLE 2. Centrifugal overload test results.

Sample number	Centrifugal acceleration /g	Head latch position	Deformation of microspring
1	2000	The head latch is locked by the cassette latch	Plastic deformation
2	1900	The head latch is locked by the cassette latch	Plastic deformation
3	1800	The head latch is locked by the cassette latch	Plastic deformation
4	1700	The head latch is locked by the cassette latch	Plastic deformation
5	1600	The head latch is locked by the cassette latch	Plastic deformation
6	1500	The head latch is locked by the cassette latch	Plastic deformation
7	1400	The head latch is locked by the cassette latch	Plastic deformation
8	1300	The head latch enters the cassette latch and grips one tooth	Plastic deformation
9	1200	Initial position	Initial state
10	1100	Initial position	Initial state

When the stress of the upper end of the spring is greater than the yield limit of nickel, plastic deformation occurs [38]. In addition, although the weight of the microspring is small, the influence of the inertial force caused by the weight of the spring on the deformation of the microspring cannot be ignored under high-overload impact. Currently, the upper end of the microspring not only bears the weight of the setback slider but also bears the weight of the entire spring, which also causes plastic deformation.

C. CENTRIFUGAL OVERLOAD TEST RESULTS

The centrifugal testing machine shown in Fig. 9 was used to simulate the firing test, and the centrifugal force generated by the testing machine was used to simulate the setback force during launch. To determine the critical centrifugal acceleration at which the setback arming device was fully released, a total of 10 tests were conducted. Prior to the test, the shear pin was artificially interrupted, and the MEMS S&A device was fixed in a specified position with respect to the testing machine. After the centrifugal acceleration was increased to the predetermined g value during the test, the MEMS S&A device was taken out after 8 seconds to observe whether the setback slider moved to the fully released position. The test

FIGURE 9. Centrifugal testing machine.

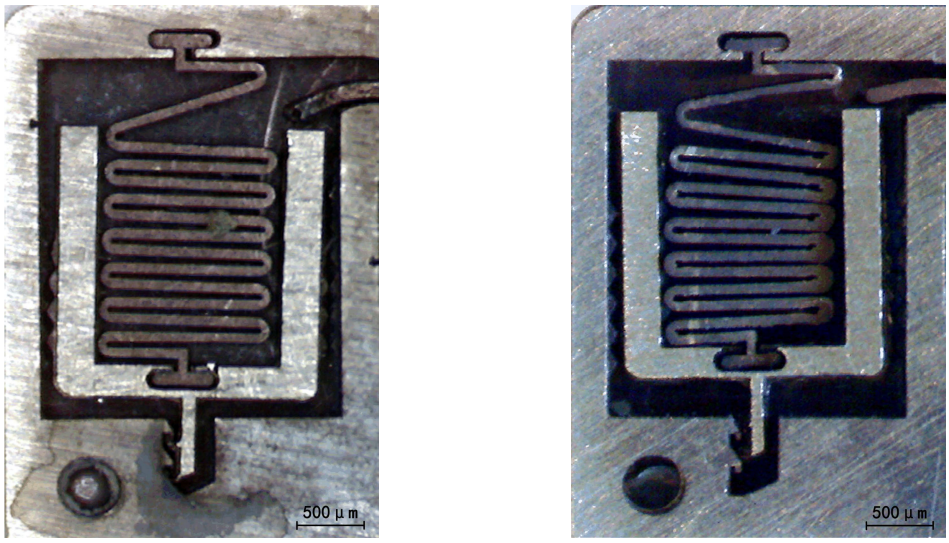

(a) (b)

FIGURE 10. Centrifugal overload test results. (a) Centrifugal acceleration of 1400 g; (b) centrifugal acceleration of 1300 g.

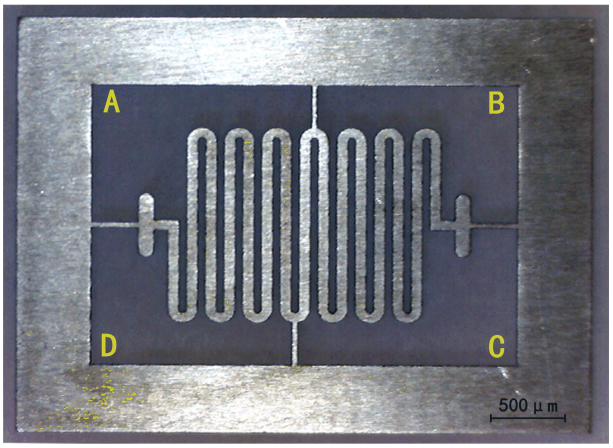

FIGURE 11. Processing scheme for the microsprings.

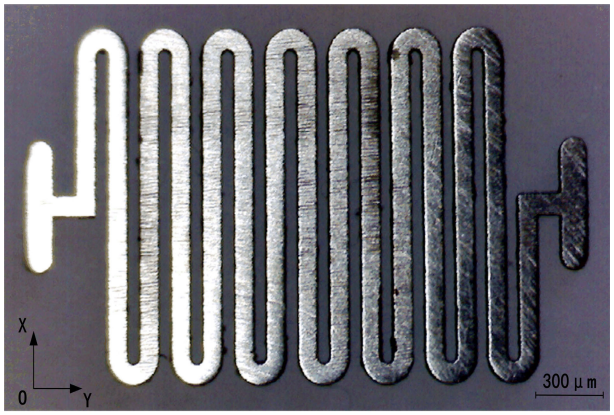

FIGURE 12. Microsprings obtained from the EDM process.

results are shown in Table 2. When the centrifugal acceleration decreased from 2000 g to 1400 g, the head latch was locked by the cassette latch, and the microspring underwent plastic deformation. At that time, although the setback arming device could completely release the insurance, the plastic deformation of the microspring may have caused the setback slider to be unable to move in place at the specified time. When the centrifugal acceleration was reduced to 1300 g, the head latch entered the cassette latch and gripped one tooth, and the microspring also underwent plastic deformation. When the centrifugal acceleration decreased from 1200 g to 1100 g, the setback slider was in the initial position, and the microspring was in the initial state. Because the high-speed camera cannot be used on the centrifugal testing machine, it is not possible to judge whether the setback slider moved under the condition of this acceleration. Fig. 10 shows an SEM image of the setback arming device at centrifugal accelerations of 1400 g and 1300 g; the upper end of the microsprings is found to undergo a large plastic deformation. The results of the centrifugal overload test show that the setback arming device cannot guarantee the reliability of the launch.

IV. OPTIMIZATION OF THE SETBACK ARMING DEVICE

A. OPTIMIZATION OF THE PROCESSING TECHNOLOGY

According to the test results shown in Fig. 6, the fabrication errors of the UV-LIGA process have a great influence on the microspring elastic coefficient, which further affects the safety and reliability of the setback arming device. Therefore, through technology research, this paper explores a high-precision and low-cost fabrication process of a MEMS S&A device: low-speed wire electrical discharge machining (EDM). As a flexible noncontact machining technology with strong advantages involving material

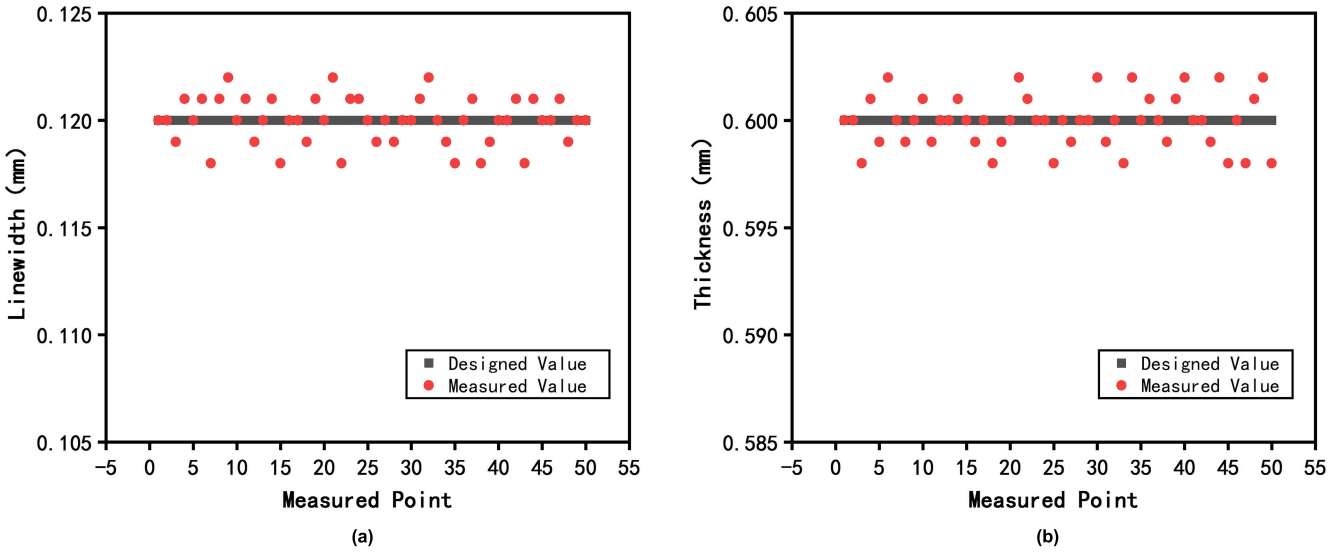

FIGURE 13. Measurement results. (a) Linewidth; (b) thickness.

TABLE 3. Fabrication errors of characteristic dimensions.

Characteristic dimension /mm	α_1	α_2	a_1	a_2	b_1	b_2
Designed value	30°	30°	0.135	0.102	0.983	0.358
UV-LIGA process measured value	38.7°	36.5°	0.181	0.156	1.012	0.464
EDM process measured value	30°	30°	0.135	0.103	0.983	0.359

TABLE 4. Mechanical impact test results.

Sample number	Peak acceleration /g	Head latch position	Deformation of microspring
1	20000	The head latch is locked by the cassette latch	Uniform deformation
2	19000	The head latch is locked by the cassette latch	Uniform deformation
3	18000	The head latch enters the cassette latch and grips one tooth, and fail to return to the initial position	Uniform deformation
4	17000	Return to the initial position	Uniform deformation
5	16000	Return to the initial position	Uniform deformation
6	15000	Return to the initial position	Uniform deformation
7	14000	Return to the initial position	Uniform deformation
8	13000	Return to the initial position	Uniform deformation
9	12000	Return to the initial position	Uniform deformation
10	11000	Return to the initial position	Uniform deformation

selection [39], [40], the EDM process has unique advantages in micropart forming by wire electrode processing and non-macro force processing [41]–[43]. By using the combined electrode fixture applied in EDM, multiple electrodes can work at the same time, which greatly improves the processing efficiency, and the machined parts have good consistency. The machine tool used for fabricating a MEMS S&A device using the EDM process is a CA20 precision slow wire EDM machine tool produced by the Azixiamir company. The machine tool can guarantee a dimensional precision of ± 2 μm, the surface roughness Ra can reach 0.03 μm, and the shape precision can be controlled within 1 μm. Copper-tungsten alloy (W75%) was used as the electrode material, and the dielectric was deionized water with a resistivity of $1 \times 10^5 \Omega$·cm. A high-purity nickel plate with a thickness of 1 mm was used as the material. The measuring device was an intelligent digital automatic stereoscopic microscope.

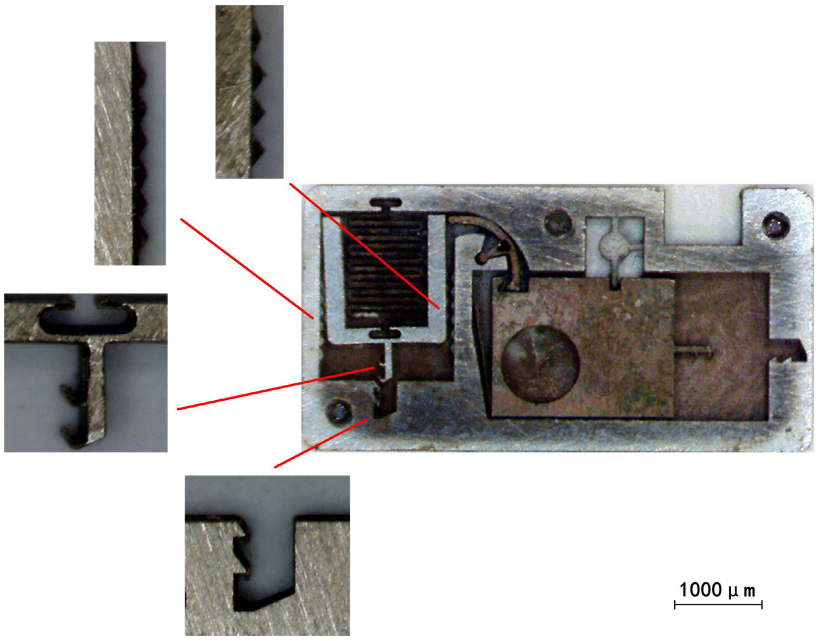

(a)

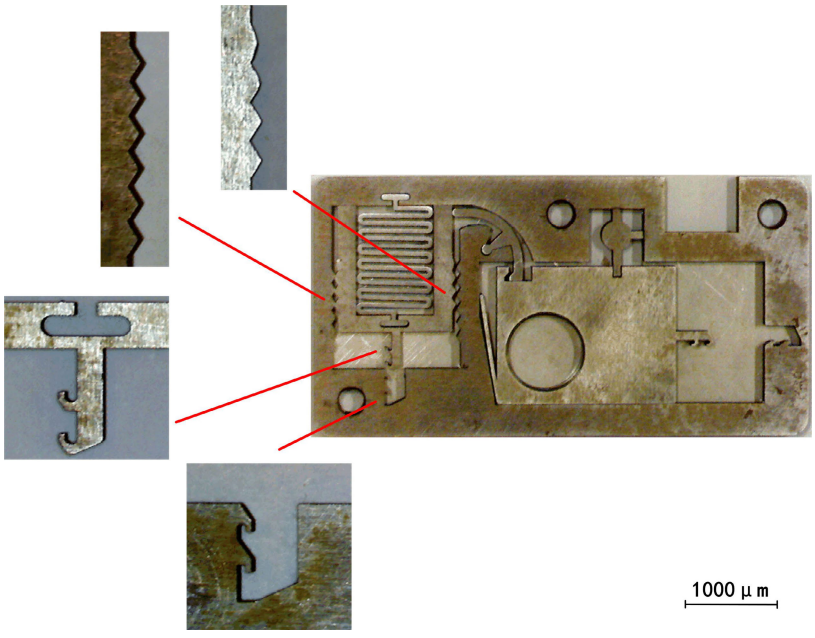

(b)

FIGURE 14. Surface morphology of the MEMS S&A device. (a) UV-LIGA process; (b) EDM process.

A microspring is difficult to fabricate using the EDM process. Due to the size effect and residual stress, the microspring is susceptible to flexural deformation and secondary deformation during processing. The machining scheme of the microspring is shown in Fig. 11. The four auxiliary supporting beam is set around the microspring, and it is found that when the width of the supporting beam is 0.04 mm, the supporting beam is ablated during cutting, preventing it from playing a supporting role. In contrast, when the width of the supporting beam is 1 mm, it takes too long to remove this beam, and the action time of the flushing pressure and the discharge reaction force increases, causing the microspring to undergo flexural deformation. Taking the above factors into consideration, it was shown by multiple tests that setting the width of the supporting beam to 0.06 mm has the least effect on the microspring. The structure shown in Fig. 11 is cut several times according to the order of A-B-C-D by using different machining allowances and machining parameters. This

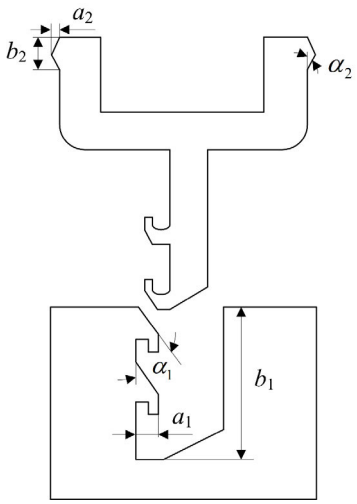

FIGURE 15. Feature dimensions of the setback arming device.

machining method can not only improve the surface quality of the microspring but also redistribute the residual stress and correct the deflection of the microspring. The microspring with an auxiliary supporting beam was then heated to 600° in a two-chamber vacuum permeable furnace for destress annealing treatment. After 2 hours, the device was placed in air to be naturally cooled. After this step, the residual stress of the microspring is smaller, and there is no secondary deformation due to the high temperature during processing. Finally, the auxiliary supporting beam is removed using the EDM process. The microspring processed by EDM is shown in Fig. 12. The microspring is not deformed, and the surface quality is good. Fifty microsprings were used to measure the linewidth and thickness of each section, and no uneven phenomena were found during the measurement. As shown in Fig. 13, compared with the microsprings fabricated using the UV-LIGA process, the measured values of the linewidth and the thickness of the microsprings fabricated with the EDM process are closer to the designed values, and the fabrication error is smaller.

Fig. 14 shows a MEMS S&A device fabricated using the UV-LIGA process and the EDM process, using 10 of each for surface topography observations and feature size measurements. It can be observed from the surface topography that the machining precision of EDM is higher for structures such as tortuous grooves, Z-shaped teeth, head latches and cassette latches. Fig. 15 shows a diagram of the characteristic dimensions of the setback arming device insurance that can be fully released. The mean value of the measured value is taken as the characteristic measurement value. The measured value is compared with the designed value. As shown in Table 3, the EDM process has a feature size closer to the designed value than the UV-LIGA process.

B. OPTIMIZATION OF THE MICROSPRING STRUCTURE

According to the test results shown in Table 1 and Table 2, the upper end of the microspring of the setback arming

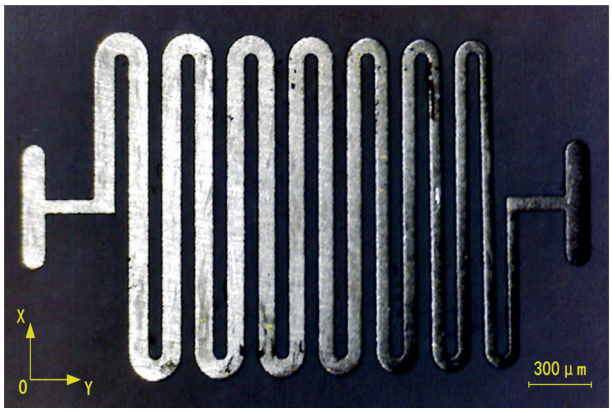

FIGURE 16. Gradient linewidth microspring.

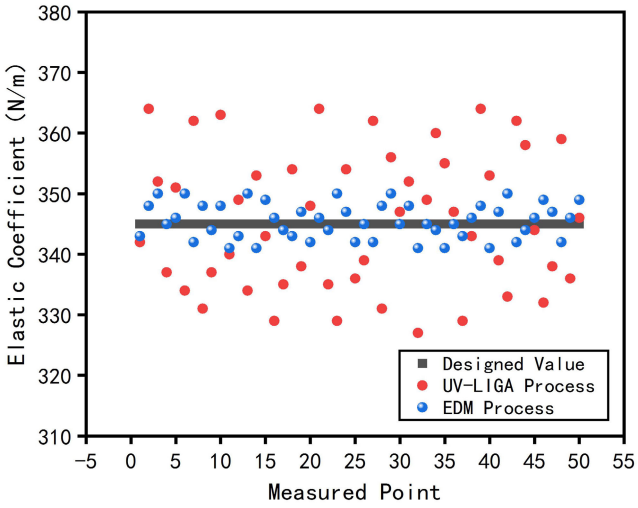

FIGURE 17. Elastic coefficient test results.

device is susceptible to large plastic deformation. Therefore, the structure of the microspring needs to be optimized. Under the same elastic coefficient of the microspring, the method of increasing the linewidth of the upper end of the spring is adopted; that is, the spring structure is designed to be a wide and narrow gradient linewidth microspring. The gradient linewidth microspring has the characteristic of resisting high overload impact, and the stress distribution of each internal section of the spring is uniform [34]. The optimized microspring structure can be determined according to the formula of the S-type gradient linewidth microspring elastic coefficient under the impact load proposed in [34]. Fig. 16 shows the gradient linewidth microspring fabricated by the EDM process with a maximum linewidth of 0.135 mm, a minimum linewidth of 0.065 mm and a linewidth increment of 0.005 mm for each straight beam. The Y-direction elastic coefficients of 50 such microsprings measured by the testing system shown in Fig. 6 are shown in Fig. 17, and the error between the measured values and the designed value is small, indicating that the EDM process has little influence on the elastic coefficients of the microsprings.

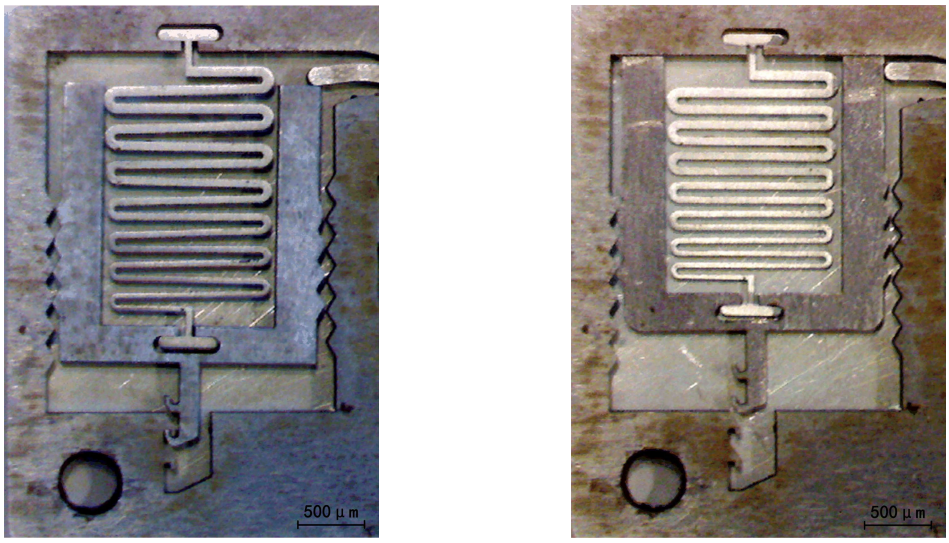

(a) (b)

FIGURE 18. Mechanical impact test results. (a) Peak acceleration of 18000 g; (b) peak acceleration of 17000 g.

TABLE 5. Centrifugal overload test results.

Sample number	Centrifugal acceleration /g	Head latch position	Deformation of microspring
1	2000	The head latch is locked by the cassette latch	Uniform deformation
2	1900	The head latch is locked by the cassette latch	Uniform deformation
3	1800	The head latch is locked by the cassette latch	Uniform deformation
4	1700	The head latch is locked by the cassette latch	Uniform deformation
5	1600	The head latch is locked by the cassette latch	Uniform deformation
6	1500	The head latch is locked by the cassette latch	Uniform deformation
7	1400	The head latch enters the cassette latch and grips one tooth	Uniform deformation
8	1300	Initial position	Initial state
9	1200	Initial position	Initial state
10	1100	Initial position	Initial state

V. TESTS OF THE OPTIMIZED SETBACK ARMING DEVICE

A. MECHANICAL IMPACT TEST RESULTS

The optimized setback arming device was subjected to a mechanical impact test under the same test conditions as those in Table 1, and the test results are shown in Table 4. The gradient linewidth microspring made by the EDM process was uniformly deformed in the mechanical impact test. When the peak acceleration decreased from 20000 g to 19000 g, the head latch was locked by the cassette latch and could not return to the initial position. When the peak acceleration was reduced to 18000 g, the head latch entered the cassette latch and gripped one tooth and could not return to the initial position. When the peak acceleration decreased from 17000 g to 11000 g, the head latch entered the cassette latch and then exited smoothly and finally returned to the initial position. Fig. 18 shows an SEM image of the setback arming device at peak accelerations of 18000 g and 17000 g; no plastic deformation can be identified at the upper end of the microspring. The mechanical impact test results show that the optimized setback arming device can ensure the safety of service processing, and the maximum overload that can be withstood in service processing is 17000 g.

B. CENTRIFUGAL OVERLOAD TEST RESULTS

A centrifugal overload test was carried out on the optimized setback arming device to ensure that the test conditions were the same as those in Table 2, and the test results are shown in Table 5. When the centrifugal acceleration decreased from 2000 g to 1500 g, the setback slider moved to the fully released position, and the deformation of the microspring was uniform. When the centrifugal acceleration was reduced to 1400 g, the head latch entered the cassette latch and gripped one tooth, and the deformation of the microspring was also uniform. When the centrifugal acceleration decreased from 1300 g to 1100 g, the setback slider was in the initial position, and the microspring was in the initial state. Fig. 19 shows

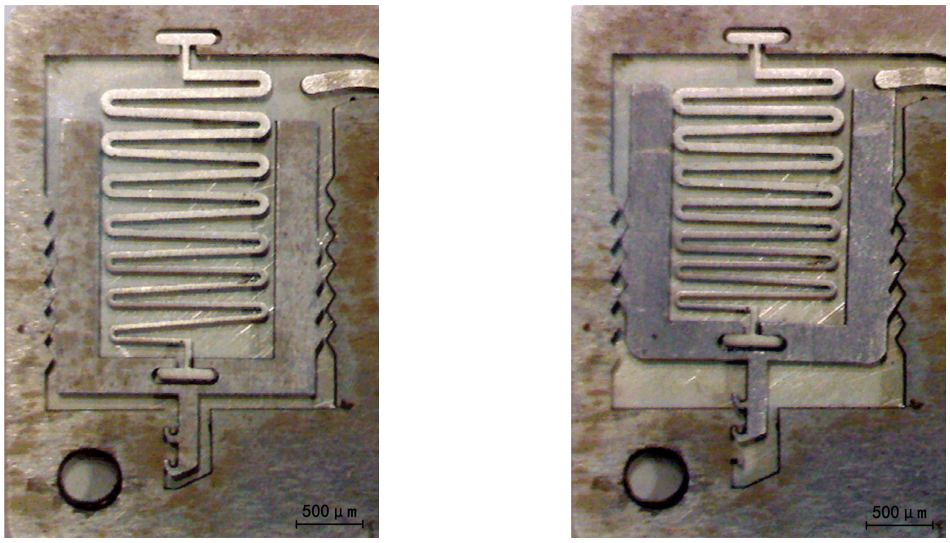

(a) (b)

FIGURE 19. Centrifugal overload test results. (a) Centrifugal acceleration of 1500 g; (b) centrifugal acceleration of 1400 g.

an SEM image of the setback arming device at centrifugal accelerations of 1500 g and 1400 g; no plastic deformation can be identified at the upper end of the microsprings. The results of the centrifugal overload test show that the optimized setback arming device can ensure the reliability of the launch, and the minimum overload for releasing the insurance during the launch is 1500 g.

VI. CONCLUSION

In this paper, a MEMS setback arming device fabricated using a UV-LIGA process is measured and tested. According to the results of measurements and tests, optimization is carried out on the two aspects of the fabrication process and the microspring structure, and a mechanical impact test and centrifugal overload test are carried out on the optimized structure. The main conclusions are as follows:

(1)The MEMS S&A device fabricated by the EDM process can reduce the machining cost and greatly improve the machining accuracy and yield relative to the characteristics and limitations of the current UV-LIGA process.

(2) The problem of flexure deformation and secondary deformation of the microspring in the EDM process can be solved by setting an auxiliary supporting beam, using multiple cuts and destress annealing. When the width of the supporting beam is 0.06 mm, the influence on the microspring is minimized.

(3) The gradient linewidth microspring structure can solve the plastic deformation problem of the upper end of the microspring after the high overload impact, and the optimized setback arming device can reliably distinguish between the service processing environment and the launch environment. The maximum overload that can be withstood in service processing is 17000 g, and the minimum overload for releasing insurance during launch is 1500 g.

REFERENCES

[1] H. Pezous, C. Rossi, M. Sanchez, F. Mathieu, X. Dollat, S. Charlot, L. Salvagnac, and V. Conédéra, "Integration of a MEMS based safe arm and fire device," *Sens. Actuators A, Phys.*, vol. 159, no. 2, pp. 157–167, May 2010.

[2] J.-H. Jeong, J. Eom, S. S. Lee, D. W. Lim, Y. I. Jang, K. W. Seo, S. S. Choi, C. J. Lee, and J. S. Oh, "Miniature mechanical safety and arming device with runaway escapement arming delay mechanism for artillery fuze," *Sens. Actuators A, Phys.*, vol. 279, pp. 518–524, Aug. 2018.

[3] D. Cigdem, M. Kadir, M. N. Hayi, and C. Omer, "Bending response of nanobeams resting on elastic foundation," *J. Appl. Comput. Mech.*, vol. 2, no. 4, pp. 105–114, Apr. 2018.

[4] M. Mohammad, "Buckling analysis of a micro composite plate with nano coating based on the modified couple stress theory," *J. Appl. Comput. Mech.*, vol. 4, no. 1, pp. 1–15, Aug. 2018.

[5] M. Deeds, P. Sandborn, and R. Swaminathan, "Packaging of a MEMS based safety and arming device," in *Proc. 7th Intersoc. Conf. Thermal Thermomech. Phenomena Electron. Syst. (ITHERM)*, Las Vegas, NV, USA, 2000, pp. 107–112.

[6] Y. Alireza, Y. Mojtaba, R. Mehran, and K. Ali, "Scale-dependent dynamic behavior of nanowire-based sensor in accelerating field," *J. Appli. Comput. Mech.*, vol. 5, no. 2, pp. 486–497, Dec. 2019.

[7] L. Fan, H. Last, R. Wood, B. Dudley, C. Khan Malek, and Z. Ling, "SLIGA based underwater weapon safety and arming system," *Microsyst. Technol.*, vol. 4, no. 4, pp. 168–171, Jul. 1998.

[8] S. Gbeminiyi, "Free convection flow and heat transfer of nanofluids of different shapes of nano-sized particles over a vertical plate at low and high Prandtl numbers," *J. Appli. Comput. Mech.*, vol. 5, no. 1, pp. 13–39, Oct. 2019.

[9] T. Hu, Y. Zhao, Y. Zhao, and W. Ren, "Integration design of a MEMS based fuze," *Sens. Actuators A, Phys.*, vol. 268, no. 1, pp. 193–200, Dec. 2017.

[10] D. K. Wang, W. Z. Lou, Y. Feng, and F. F. Wang, "Parametric study of the centrifugal insurance mechanism in MEMS safety and arming device," *Eur. PMC*, vol. 257, no. 1, pp. 1–11, Mar. 2017.

[11] G. Subramanian, M. Deeds, K. R. Cochran, R. Raghavan, and P. A. Sandborn, "Delamination study of chip-to-chip bonding for a LIGA-based safety and arming system," *Proc. SPIE*, vol. 3880, pp. 111–119, Aug. 1999.

[12] W. Fufu, L. Wenzhong, X. Yongjia, L. Fangyi, W. Dakui, J. Xin, Z. Mingrong, and X. Chenggang, "The parametric analysis of the centrifugal insurance mechanism in MEMS safety and arming device," in *Proc. 10th IEEE Int. Conf. Nano/Micro Engineered Mol. Syst.*, Xi'an, China, Apr. 2015, pp. 456–460.

[13] R. Swati, S. P. Duttagupta, and H. Mutthurajan, "MEMS based spin sensor displacement analysis in nanometer precision using COMSOL for S&A devices," in *Proc. 3rd Int. Conf. Devices, Circuits Syst. (ICDCS)*, Coimbatore, India, Mar. 2016, pp. 78–83.
[14] H. Zhang, Y. Wang, W. Z. Lou, F. Y. Liu, and F. F. Wang, "Reliability factors analysis of MEMS safety and arming system," *Key Eng. Mater.*, vols. 609–610, pp. 1494–1497, Apr. 2014.
[15] W. Fufu, L. Wenzhong, F. Yue, and W. Ying, "Parametric research of MEMS safety and arming system," in *Proc. 8th Annu. IEEE Int. Conf. Nano/Micro Engineered Mol. Syst.*, Jiangsu, China, Apr. 2013, pp. 767–770.
[16] W. Dakui, L. Wenzhong, X. Yongjia, W. Fufu, L. Fangyi, J. Xin, and L. Jun, "The effect of micro-spring stiffness changes on the typical MEMS S&A device," in *Proc. 10th IEEE Int. Conf. Nano/Micro Engineered Mol. Syst.*, Xi'an, China, Apr. 2015, pp. 413–416.
[17] H. M. Tu, Z. L. Sun, Y. P. Qian, and Q. Liu, "Reliability analysis and improvement of MEMS-based safety and arming device in fuze," *Acta Armamentarii*, vol. 38, no. 4, pp. 664–672, Apr. 2017.
[18] J. O. Seok, J.-H. Jeong, J. Eom, S. S. Lee, C. J. Lee, S. M. Ryu, and J. S. Oh, "Ball driven type MEMS SAD for artillery fuse," *J. Micromech. Microeng.*, vol. 27, no. 1, Jan. 2017, Art. no. 015032.
[19] H. Li and G. C. Shi, "Contrastive study on the mechanical performance of MEMS microsprings fabricated by LIGA and UV-LIGA technology," *MEMS/MOEMS Technol. Appl. III*, vol. 6836, Jan. 2008, Art. no. 68360E.
[20] L. Du, "Fabrication of fuze Micro-electro-mechanical system safety device," *Chin. J. Mech. Eng.*, vol. 24, no. 5, pp. 836–841, Jan. 2011.
[21] R. A. Lawes, "Manufacturing tolerances for UV LIGA using SU-8 resist," *J. Micromech. Microeng.*, vol. 15, no. 11, pp. 2198–2203, Nov. 2005.
[22] L. Q. Du, A. A. Wang, M. Zhao, and M. C. Song, "The fabrication of trans-scale micro-fuze safety device," *Key Eng. Mater.*, vols. 609–610, pp. 796–800, Apr. 2014.
[23] B. L. Kistler, A. S. Dryden, J. A. W. Crowell, and S. K. Griffiths, "Dimensional errors in LIGA-produced metal structures due to thermal expansion and swelling of PMMA," *J. Micromech. Microeng.*, vol. 14, no. 11, p. 1548, 2004.
[24] H. Hossein and H. Mojtaba, "Elastic-plastic analysis of bending moment—Axial force interaction in metallic beam of T-section," *J. Appl. Comput. Mech.*, vol. 5, no. 1, pp. 162–173, Mar. 2019.
[25] J. D. Williams and W. Wang, "Microfabrication of an electromagnetic power relay using SU-8 based UV-LIGA technology," *Microsyst. Technol.*, vol. 10, no. 10, pp. 699–705, Dec. 2004.
[26] H.-K. Chang and Y.-K. Kim, "UV-LIGA process for high aspect ratio structure using stress barrier and C-shaped etch hole," *Sens. Actuators A, Phys.*, vol. 84, no. 3, pp. 342–350, Sep. 2000.
[27] L. Yi, W. Xiaodong, L. Chong, L. Zhifeng, C. Denan, and Y. Dehui, "Swelling of SU-8 structure in ni mold fabrication by UV-LIGA technique," *Microsyst. Technol.*, vol. 11, no. 12, pp. 1272–1275, Nov. 2005.
[28] M. Alborz and M. Reza, "A note on free vibration of a double-beam system with nonlinear elastic inner layer," *J. Appli. Comput. Mech.*, vol. 5, no. 1, pp. 174–180, Feb. 2019.
[29] C. K. Chung, K. L. Sher, Y. J. Syu, and C. C. Cheng, "Fabrication of cone-like microstructure using UV LIGA-like for light guide plate application," *Microsyst. Technol.*, vol. 16, nos. 8–9, pp. 1619–1624, Aug. 2010.
[30] C.-H. Lin, G.-B. Lee, B.-W. Chang, and G.-L. Chang, "A new fabrication process for ultra-thick microfluidic microstructures utilizing SU-8 photoresist," *J. Micromech. Microeng.*, vol. 12, no. 5, pp. 590–597, Sep. 2002.
[31] L. Du, M. Zhao, A. Wang, S. Chen, and W. Nie, "Fabrication of novel MEMS inertial switch with six layers on a metal substrate," *Microsyst. Technol.*, vol. 21, no. 9, pp. 2025–2032, Sep. 2015.
[32] W. Dai, C. Oropeza, K. Lian, and W. Wang, "Experiment design and UV-LIGA microfabrication technology to study the fracture toughness of Ni microstructures," *Microsyst. Technol.*, vol. 12, no. 4, pp. 306–314, Mar. 2006.
[33] Y. Qin, L. Chen, Y. Hao, S. Liu, and X. Zou, "A study on the elastic coefficients of setback micro-springs for a MEMS safety and arming device," *Microsyst. Technol.*, vol. 26, no. 2, pp. 583–593, Feb. 2020.
[34] W. Nie, J. Cheng, Z. Xi, Z. Zhou, and L. Yin, "Elastic coefficient analysis on planar S-shaped micro spring under high impact load," *Microsyst. Technol.*, vol. 23, no. 5, pp. 1367–1375, May 2017.
[35] J. K. Liu, X. L. Qi, X. F. Wang, and L. Xu, "Reliability enhancement test technology of fuse MEMS mechanism," *J. Detective Control*, vol. 35, no. 3, pp. 41–45, Jun. 2013.
[36] J. K. Liu and N. Li, "Failure models of MEMS setback arming device under high impact environment," *J. Detective Contro.*, vol. 38, no. 6, pp. 15–19, Dec. 2016.
[37] J. K. Liu, X. L. Qi, R. G. Zhu, and H. Li, "The problem of MEMS setback arming device and resolution," *J. Projectiles, Rockets, Missiles Guid.*, vol. 33, no. 3, pp. 63–69, Jun. 2013.
[38] G. Z. Li, "Research on micro safe and arming system," Ph.D. dissertation, Beijing Inst. Technol., Beijing, China, 2016.
[39] Y. Gong, Y. Sun, X. Wen, C. Wang, and Q. Gao, "Experimental study on surface integrity of Ti-6Al-4 V machined by LS-WEDM," *Int. J. Adv. Manuf. Technol.*, vol. 88, nos. 1–4, pp. 197–207, Jan. 2017.
[40] Y. Gong, Y. Su, J. Cheng, C. Wang, Y. Liu, and Z. Zhu, "Modeling and experimental study on breakdown voltage (BV) in low speed wire electrical discharge machining (LS-WEDM) of Ti-6Al-4 V," *Int. J. Adv. Manuf. Technol.*, vol. 90, nos. 5–8, pp. 1277–1292, May 2017.
[41] R. Mukherjee, S. Chakraborty, and S. Samanta, "Selection of wire electrical discharge machining process parameters using non-traditional optimization algorithms," *Appl. Soft Comput.*, vol. 12, no. 8, pp. 2506–2516, Apr. 2012.
[42] B. Kuriachen, K. P. Somashekhar, and J. Mathew, "Multiresponse optimization of micro-wire electrical discharge machining process," *Int. J. Adv. Manuf. Technol.*, vol. 76, nos. 1–4, pp. 91–104, Jan. 2015.
[43] A. Aref Arjmand, S. Khalaj Amineh, H. Salimijazi, and A. Fadaei Tehrani, "Etch assisted ultrasonic floating abrasion process, a new concept for material removal," *Microelectron. Eng.*, vol. 129, pp. 31–37, Nov. 2014.

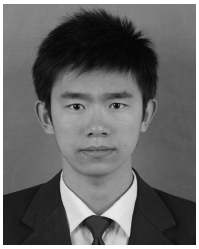

YU QIN was born in Dandong, Liaoning, China, in 1990. He received the M.E. degree in mechanical engineering from Dalian Jiaotong University, Dalian, China, in 2015. He is currently pursuing the Ph.D. degree in mechanical engineering with Northeastern University, Shenyang, China.

His research interests include the application of micro-springs, and the design of MEMS safety and arming device.

LIANGYU CHEN was born in Weifang, Shandong, China, in 1959. He received the B.E. degree in mechanical engineering from the China University of Petroleum, Dongying, China, in 1982, and the M.E. and Ph.D. degrees in mechanical engineering from Northeastern University, Shenyang, China, in 1986 and 1994, respectively.

Since 1997, he has been a Professor with the School of Mechanical Engineering and Automation, Northeastern University. He is the author of 12 books and more than 80 articles. His research interests include structural integrity of metallurgical equipment, mechanical power transmission and transmission technology, and engineering equipment modeling and digital technology.

YONGPING HAO was born in Shenyang, Liaoning, China, in 1960. He received the Ph.D. degree in mechanical engineering from the Beijing Institute of Technology, Beijing, China, in 2004.

He is currently a Professor with Shenyang Ligong University. His research interests include applied information technology and microsystems application technology.